

Available online at [www.synsint.com](http://www.synsint.com)

# Synthesis and Sintering

ISSN 2564-0186 (Print), ISSN 2564-0194 (Online)



Research article

## Oxidation-affected zone in the sintered $ZrB_2$ -SiC-HfB<sub>2</sub> composites



Ebrahim Dodi , Zohre Balak \*, Hosein Kafashan

Department of Materials Science and Engineering, Ahvaz Branch, Islamic Azad University, Ahvaz, Iran

### ABSTRACT

Understanding the behavior of ultra-high temperature ceramics (UHTCs) against oxidation is of particular importance in high-temperature applications. In this study,  $ZrB_2$ -SiC-HfB<sub>2</sub> UHTC composites were fabricated by spark plasma sintering (SPS) method at different temperatures, times, and pressures to investigate the effects of sintering process variables on their oxidation resistance. Before the oxidation tests, the as-sintered samples contained  $ZrB_2$  and SiC phases with (Zr,Hf)B<sub>2</sub> solid solution. The samples were subjected to oxidative conditions at 1400 °C and their relative mass changes were measured as a function of oxidation time up to 20 hours. FESEM and EDS equipment were used for microstructural and elemental analyzes of cross-sections of different oxide layers. Due to the oxygen diffusion, ZrO<sub>2</sub> and SiO<sub>2</sub> phases appeared alongside (Zr,Hf)O<sub>2</sub> in the surface layers. After identifying the several oxides and SiC-depleted layers in the oxidation-affected zone, a schematic model for the arrangement of such layers was proposed.

© 2022 The Authors. Published by Synsint Research Group.

### KEYWORDS

UHTCs  
 $ZrB_2$ -SiC-HfB<sub>2</sub>  
 Oxidation resistance  
 SPS  
 Oxide layers  
 SiC-depleted area



### 1. Introduction

Zirconium diboride as a member of a group of materials named ultra-high temperature ceramics (UHTCs) has a melting point of more than 3000 °C [1–4]. This ceramic has gained great interest in structural applications, in particular for the protection of hypersonic aerospace sector exposed to environments with high flow of hot oxidizing gases [5–7]. Besides, the unique combination of properties like low electrical resistivity, high thermal conductivity, high flexural strength, and relatively low density has made  $ZrB_2$  a promising candidate for other applications including furnace electrodes, microelectronics, cutting tools, metal crucibles, and solar collectors [8–11].

In addition to the mentioned characteristics, SiC-reinforced  $ZrB_2$ -based materials exhibit additional favorable properties [12–14]. Flexural strength above 1000 MPa [15, 16], hardness in excess of 22 GPa [17, 18], and fracture toughness of 5.5 MPa.m<sup>1/2</sup> [19, 20] can be obtained by introduction of SiC to  $ZrB_2$  ceramic. Oxidation rate of

underlying  $ZrB_2$  can be slowed by forming a borosilicate glassy film on the surface

using SiC additives [21, 22]. These obtained results have led to  $ZrB_2$ -SiC composites being investigated by several researchers for advanced applications [23–26].

Recently, introduction of different kinds of sintering aids to UHTCs is as an approach to obtain improved high-temperature performance [27–29]. Several researches were performed on improvement of oxidation resistance of  $ZrB_2$ -based composites in high-temperature applications. Temperature is a critical factor in oxidation of  $ZrB_2$  when it is exposed to an oxidizing atmosphere. The oxidation behavior of monolithic  $ZrB_2$  was examined in a broad temperature range from 500 to 1500 °C. Above 550 °C, heating the sample led to the formation of a smooth and golden-bluish layer, composed of B<sub>2</sub>O<sub>3</sub> [30]. Evaporation of B<sub>2</sub>O<sub>3</sub> above 1370 °C led to an increase in the oxidation rate of  $ZrB_2$  [31]. Oxidation rate is a function of thermodynamic parameters such as partial pressure of B<sub>2</sub>O<sub>3</sub> and oxygen pressure [32].

\* Corresponding author. E-mail address: [z.balak@iauhvaz.ac.ir](mailto:z.balak@iauhvaz.ac.ir), [zbalak1983@gmail.com](mailto:zbalak1983@gmail.com) (Z. Balak)

Received 6 March 2022; Received in revised form 25 March 2022; Accepted 26 March 2022.

Peer review under responsibility of Synsint Research Group. This is an open access article under the CC BY license (<https://creativecommons.org/licenses/by/4.0/>).  
<https://doi.org/10.53063/synsint.2022.21111>

**Table 1.** Composition and sintering parameters of ZrB<sub>2</sub>-based composites prepared by SPS method.

Sample no.	Secondary phases		SPS parameters		
	SiC (vol%)	HfB <sub>2</sub> (vol%)	Temperature (°C)	Time (min)	Pressure (MPa)
1	30	12	1650	9	30
2	30	12	1725	9	30
3	30	12	1800	9	30
4	30	8	1725	4	20
5	30	8	1725	9	20
6	30	8	1725	14	20
7	30	8	1725	9	30
8	30	8	1725	9	40

Adding SiC, Si<sub>3</sub>N<sub>4</sub>, and ZrC to ZrB<sub>2</sub> for enhancing the oxidation resistance has been attempted. Among the mentioned additives, SiC has gained researchers attention owing to decrease in oxidation rate because of the ability of this carbide to form SiO<sub>2</sub> scales at temperatures above 1200 °C [33–39]. Preferential oxidation of SiC led to the formation of a porous ZrB<sub>2</sub> zone, named SiC-depleted layer, under the SiO<sub>2</sub>-rich layer [40]. Influence of SiC amount on the oxidation behavior of ZrB<sub>2</sub> at 1800 °C was evaluated. Formation of ZrO<sub>2</sub>-contained SiO<sub>2</sub> layers was observed owing to evaporation of liquid SiO<sub>2</sub> on the surface and appearance of ZrO<sub>2</sub> below the SiO<sub>2</sub> layer [41].

In this paper, the effects of spark plasma sintering parameters (temperature, time, and pressure) on the oxidation behavior of ZrB<sub>2</sub>-SiC-HfB<sub>2</sub> composites are studied. Field emission scanning electron microscopy (FESEM) and energy dispersive spectroscopy (EDS) are employed for microstructural and chemical (elemental) analyses of the different oxidation-affected layers formed after oxidation tests.

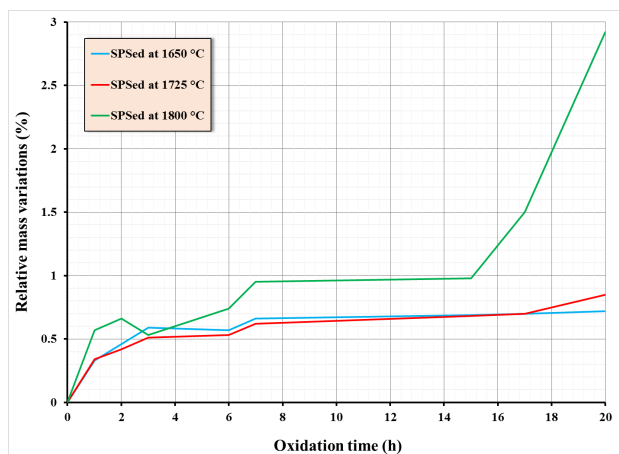


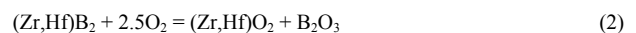
**Fig. 1.** Relative mass variations as a function of oxidation time in the ZrB<sub>2</sub>-30 vol% SiC-12 vol% HfB<sub>2</sub> composites oxidized at 1400 °C, which had been sintered for 9 min under 30 MPa at 1650, 1725, and 1800 °C.

## 2. Experimental procedure

Commercially available SiC (particle size: 15 μm, purity: 98.7%), HfB<sub>2</sub> (particle size: 20 μm, purity: 98.7%), and ZrB<sub>2</sub> (particle size: 20 μm, purity: 99.5%) powders were purchased from Northwest Institute for Non-Ferrous Metal Research (China) as the starting ceramic materials. Eight composite samples were prepared according to the composition and spark plasma sintering conditions presented in Table 1. The powders were weighed and mixed by wet ball-milling for 3 h at 250 rpm in ethanol employing tungsten carbide cup and balls. The powder mixtures were dried on a magnet heater and then loaded into graphite molds designed for sintering purposes. Sintering process was carried out by spark plasma sintering technology (SPS: 20T-10, China). The sintered disk-shaped composites were ground to remove the attached graphite foils and then prepared by machining (EDM technology) for oxidation test. The oxidation tests were carried out using a box furnace for 1, 2, 3, 6, 7, 15, 17, and 20 h at a fixed temperature of 1400 °C. The relative mass change was calculated as the oxidation criterion, as a result of dividing the mass variation due to oxidation by the initial mass. Microstructural and elemental (chemical) analyses were performed using Tescan Mira3 FESEM apparatuses equipped with EDS facility.

## 3. Results and discussion

Microstructural studies of sintered samples, the findings of which have already been published in Ref. [21], showed that the composites are generally made of dark gray grains of the ZrB<sub>2</sub> matrix, black SiC secondary phases, and light gray grains of (Zr,Hf)B<sub>2</sub> solid solution. If the mentioned composites are subjected to oxidation testing at 1400 °C, the phases and grains in their microstructures must be oxidized according to the following reactions:



Our preliminary studies proved that the addition of HfB<sub>2</sub> and also

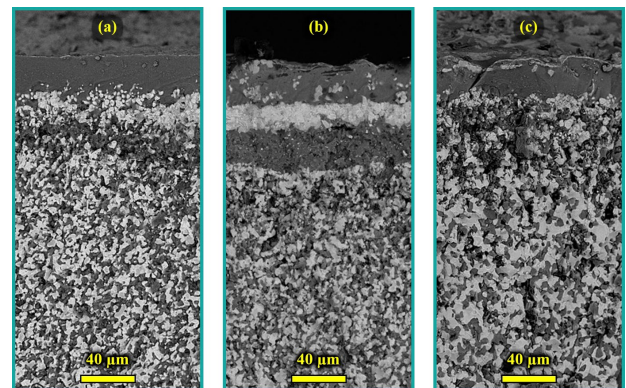


**Fig. 2.** Cross-sectional FESEM images of the oxidized ZrB<sub>2</sub>-30 vol% SiC-12 vol% HfB<sub>2</sub> composites at 1400 °C for 20 h, which had been sintered for 9 min under 30 MPa at a) 1650 °C, b) 1725 °C, and c) 1800 °C.

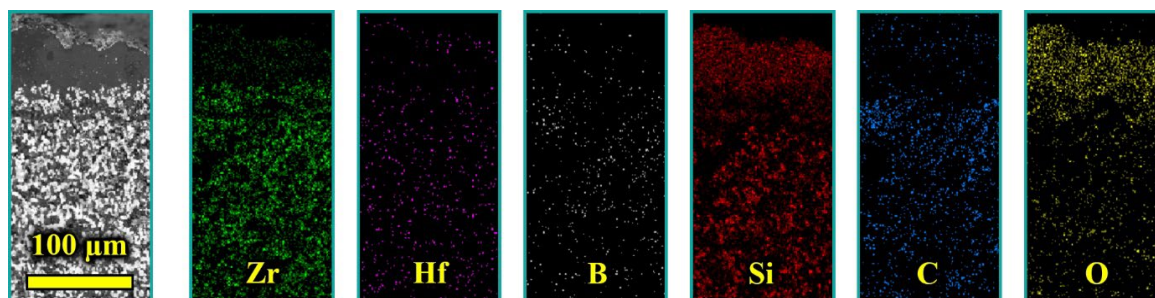


**Fig. 3.** Cross-sectional EDS map analysis of the oxidized  $\text{ZrB}_2$ –30 vol% SiC–12 vol%  $\text{HfB}_2$  composites at 1400 °C for 20 h, which had been sintered at 1650 °C for 9 min under 30 MPa.

increasing its amount can boost the oxidation resistance of  $\text{ZrB}_2$  matrix composites. In fact, oxidation resistance of  $\text{ZrB}_2$  is lower than  $\text{HfB}_2$  due to volumetric changes during the  $\text{ZrO}_2$  phase transformation as well as less oxygen diffusion in  $\text{HfO}_2$  than in  $\text{ZrO}_2$ . Therefore, the presence of  $\text{HfB}_2$  improves the oxidation resistance of  $\text{ZrB}_2$ –SiC composite [21]. Meanwhile, SiC reinforcement in  $\text{ZrB}_2$ - and  $\text{HfB}_2$ -based ceramics forms  $\text{B}_2\text{O}_3$ – $\text{SiO}_2$  glassy layer during oxidation, which is more viscous and stable compared to  $\text{B}_2\text{O}_3$  and has lower vapor pressure. Oxygen cannot penetrate easily in such an amorphous  $\text{SiO}_2$ -rich layer due to its high viscosity, and as a result, the composite remains resistant to oxidizing environments at least up to 1600 °C. However, the viscosity of this layer is not so high that it cannot fill the pores and discontinuities in  $\text{ZrO}_2$  and  $\text{HfO}_2$ . Hence, it is possible to have a perfect coating on the sample surface due to its excellent wettability.

### 3.1. Effect of SPS temperature

To investigate the effect of sintering temperature of composites on their oxidation behavior, samples 1, 2, and 3 in Table 1 were selected for comparison. The graphs of relative mass changes over the oxidation time of these UHTCs are shown in Fig. 1. It is noteworthy that the samples had the same composition ( $\text{ZrB}_2$  matrix reinforced with 30 vol% SiC and 12 vol%  $\text{HfB}_2$ ) and underwent the same oxidation test

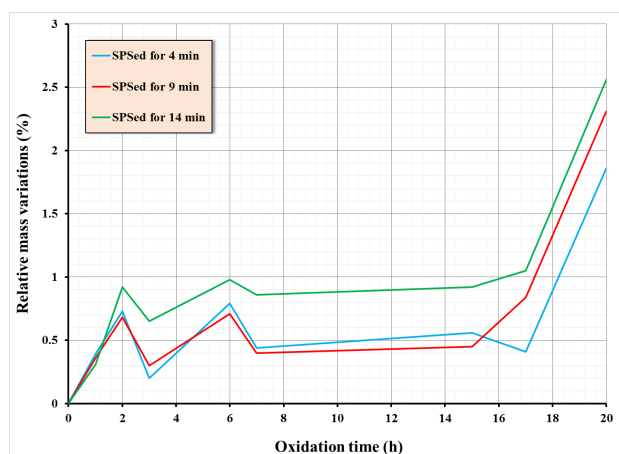


**Fig. 4.** Relative mass variations as a function of oxidation time in the  $\text{ZrB}_2$ –30 vol% SiC–8 vol%  $\text{HfB}_2$  composites oxidized at 1400 °C, which had been sintered at 1725 °C under 20 MPa for 4, 9, and 14 min.

at temperature of 1400 °C for a maximum time of 20 h. Except the SPS temperature (1650, 1725, and 1800 °C), which is the studied variable in this section, other parameters of the sintering process were considered similar (SPS time of 9 min and applied pressure of 30 MPa). Fig. 1 clearly shows that with increasing the SPS temperature from 1650 to 1725 °C, no significant changes in the oxidation trend and intensity occur, while with sintering at 1800 °C, the oxidation of the sample increases dramatically, especially from 15 h onwards.

For further investigation, cross-sectional FESEM micrographs of all samples sintered at 1650, 1725 and 1800 °C as well as EDS map images of the sample sintered at 1650 °C, after oxidation for 20 h at 1400 °C, are shown in Figs. 2 and 3, respectively. By carefully examining the figures together with the phase analyses, five distinct regions can be identified in the oxidized samples: (1) a very thin scale of  $\text{ZrO}_2$  and  $(\text{Zr,Hf})\text{O}_2$  in the outer layer in contact with the environment, (2) a significant  $\text{SiO}_2$  layer that is almost uniform and pure, (3) a layer of  $\text{SiO}_2$  mixed with  $\text{ZrO}_2$  and  $(\text{Zr,Hf})\text{O}_2$ , (4) a SiC-depleted layer, and (5) the unoxidized region where oxygen has not reached. Several papers have also shown that in SiC reinforced  $\text{ZrB}_2$ -based ceramics, the formation of  $\text{SiO}_2$  layer (according to Eq. 3) consumes the Si in the below layer, and hence, the SiC-depleted layer appears. The formed glassy layer of  $\text{SiO}_2$  is adhesive, which makes composite resistant to oxidation [22, 42].

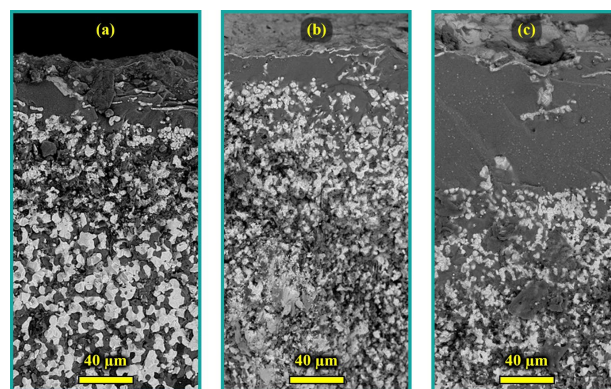


**Fig. 5.** Cross-sectional FESEM images of the oxidized  $\text{ZrB}_2$ –30 vol% SiC–8 vol%  $\text{HfB}_2$  composites at 1400 °C for 20 h, which had been sintered at 1725 °C under 20 MPa for (a) 4 min, (b) 9 min, and (c) 14 min.

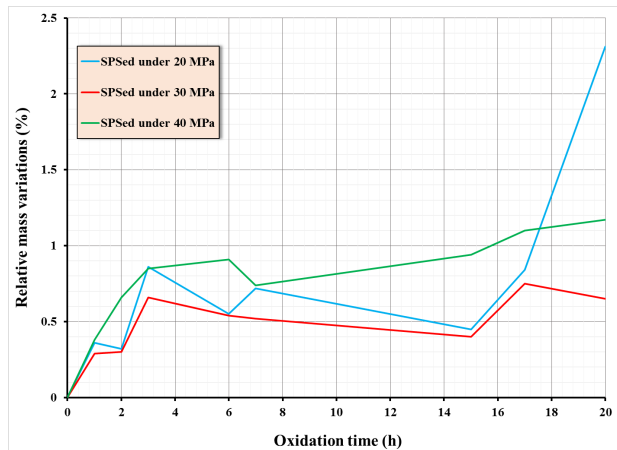


**Fig. 6.** Relative mass variations as a function of oxidation time in the  $\text{ZrB}_2$ -30 vol%  $\text{SiC}$ -8 vol%  $\text{HfB}_2$  composites oxidized at 1400 °C, which had been sintered at 1725 °C for 9 min under 20, 30, and 40 MPa.

According to the microstructures shown in Fig. 2, the total thickness of these layers is about 100  $\mu\text{m}$ . However, the thickness of the sample sintered at 1800 °C seems a little more than the other two samples. This observation is also consistent with relative mass variations as a function of oxidation time (see Fig. 1). With increasing SPS temperature from 1650 to 1725 °C, no significant mass changes occurred; therefore, the total thickness of the area affected by oxidation was not significantly different.

Preliminary microstructural studies published in Ref. [21] showed that with increasing sintering temperature from 1650 to 1725 °C, no remarkable grain growth occurred, but by sintering at 1800 °C, the grain size of  $\text{ZrB}_2$  and especially  $\text{SiC}$  increased. Therefore, the decrease in oxidation resistance at 1800 °C can be attributed to the increase in grain size.

### 3.2. Effect of SPS time

Comparison of samples 4, 5, and 6 in Table 1 was used to study the effect of SPS time on the oxidation behavior of composites. In this section, except for the soaking time at maximum processing temperature, which is the variable here; i.e. sintering for 4, 9, and 14 min, other parameters of the manufacturing process and oxidation test were kept constant. All three  $\text{ZrB}_2$  composites were fabricated with the addition of 30 vol%  $\text{SiC}$  and 8 vol%  $\text{HfB}_2$  at 1725 °C under 20 MPa

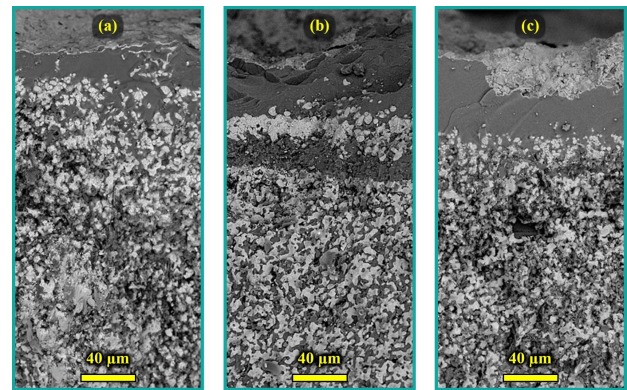


**Fig. 7.** Cross-sectional FESEM images of the oxidized  $\text{ZrB}_2$ -30 vol%  $\text{SiC}$ -8 vol%  $\text{HfB}_2$  composites at 1400 °C for 20 h, which had been sintered at 1725 °C for 9 min under a) 20 MPa, b) 30 MPa, and c) 40 MPa.

and then subjected to oxidation tests for various periods (up to 20 h) at 1400 °C.

Diagrams of relative mass changes of samples in terms of oxidation time for SPSed samples at different soaking times are plotted in Fig. 4. In general, it can be seen that increasing the soaking time of the sample at the maximum sintering temperature relatively increases the oxidation. Of course until the 15<sup>th</sup> hour, there is no significant difference in the oxidation behavior of the samples sintered for 4 and 9 min, but the increase in oxidation of the sample sintered for 14 min is significant. However, all three samples underwent severe oxidation after 15 h and there was an increasing relationship between oxidation rate and SPS time.

Microstructures of the oxidized cross-section of composites sintered at different times are shown in Fig. 5. In these images, the formation of multiple oxide layers affected by the penetration of oxygen can also be detected. According to the thickness of the resulting layers, it is concluded that the amount of oxidation is directly related to the sintering time of the samples. This is especially true when observing the significant thickness of the  $\text{SiO}_2$  layer in the sample sintered for 14 min compared to the other two samples, which were made in shorter times. In other words, increased oxidation is accompanied by thickening of the  $\text{SiO}_2$  layer. Such observations can be attributed to the grain size of  $\text{ZrB}_2$  and  $\text{SiC}$  in sintered samples. Logically, by increasing the holding time of the sample at the maximum SPS temperature, the grains grow more.

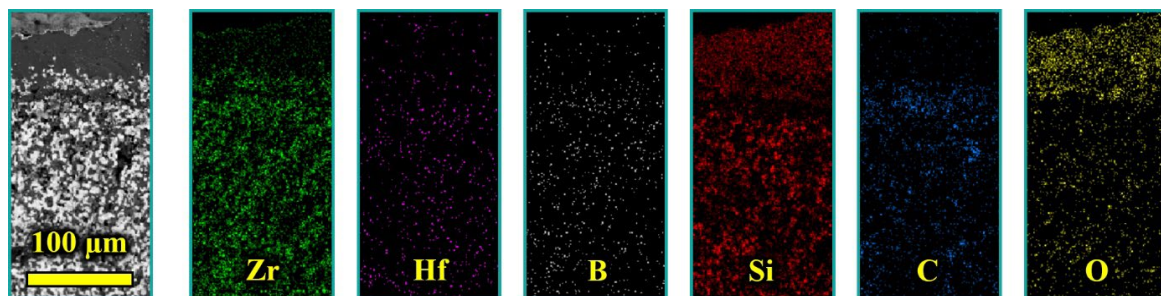


**Fig. 8.** Cross-sectional EDS map analysis of the oxidized  $\text{ZrB}_2$ -30 vol%  $\text{SiC}$ -8 vol%  $\text{HfB}_2$  composites at 1400 °C for 20 h, which had been sintered at 1725 °C for 9 min under 30 MPa.

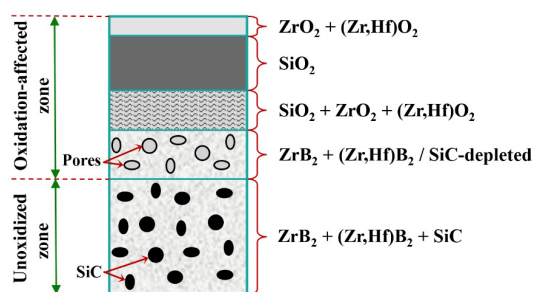


Fig. 9. Schematic of different layers formed by oxidation in  $ZrB_2$ -SiC-HfB<sub>2</sub> composites.

### 3.3. Effect of SPS pressure

In order to scrutinize the influence of SPS pressure on the oxidation rate of the composites, samples 5, 7, and 8 were selected from Table 1. All three samples, the  $ZrB_2$ -based ceramics reinforced with 30 vol% SiC and 8 vol% HfB<sub>2</sub>, had been sintered under the same temperature of 1725 °C and soaking time of 9 min but under various pressures of 20, 30, and 40 MPa. The as-sintered composites were subjected to the same oxidation test at 1400 °C for a period of 20 h. The relative mass change curves with respect to the oxidation time of the composites are plotted in Fig. 6. It can be seen that the sample sintered under the pressure of 30 MPa showed the best resistance to oxidation and the sample SPSed by applying the pressure of 20 MPa had the weakest performance. After 17 hours of oxidation, a sharp drop in oxidation resistance occurred in the sample sintered under 20 MPa.

Fig. 7 shows cross-sectional FESEM images of specimens sintered under different pressures after 20 hours of oxidation at 1400 °C. In addition, cross-sectional EDS maps of the sample SPSed under 30 MPa are shown in Fig. 8. The formation of various oxidation-affected layers is also observed here. From the comparison of the micrographs of Fig. 7, it can be clearly seen that the thickness of the oxidation-affected zone in the sample sintered under 30 MPa is much less than the two composites manufactured under pressures of 20 and 40 MPa. Microstructural studies of the sintered samples, before oxidation test, showed that the composite fabricated under 30 MPa had a finer microstructure than the other samples [21].

In the end, it is worth noting that in some microstructures, the layers were distinct and distinguishable from each other, but in some samples, such layers overlapped and precise boundaries between them were not seen. Examining the microstructures of the oxidized cross section and the values of the relative mass changes due to oxidation, it seems that the oxidation resistance was better in the samples whose oxide layers were distinct and distinguishable.

In order to better illustrate the mechanisms and arrangement of the formation of different oxidation-affected layers on the surface of  $ZrB_2$ -SiC-HfB<sub>2</sub> composites, a summary of the observations and discussions provided in this paper is shown schematically in Fig. 9.

## 4. Conclusions

The oxidation behavior of  $ZrB_2$ -SiC-HfB<sub>2</sub> composite samples manufactured at different temperatures, times and pressures by SPS method was evaluated. By comparing the cross-sectional microstructures of all composites after oxidation for 20 h at 1400 °C, it is concluded that the microstructure of the oxidation-affected zone can be divided into four layers: (1) thin scale of  $ZrO_2$  and  $(Zr,Hf)O_2$ , (2) thick uniform layer of  $SiO_2$ , (3) mixed layer of  $SiO_2$ ,  $ZrO_2$  and

$(Zr,Hf)O_2$ , and (4) SiC-depleted layer. The effects of SPS variables (temperature, time and pressure) on oxidation resistance of  $ZrB_2$ -SiC-HfB<sub>2</sub> composites were also discussed. Finally, different layers that appeared on the surface of  $ZrB_2$ -SiC-HfB<sub>2</sub> composites, due to the oxygen diffusion during the oxidation test, were schematically modeled and illustrated.

## CRedit authorship contribution statement

**Ebrahim Dodi:** Investigation, Funding acquisition.

**Zohre Balak:** Project administration, Software, Writing – original draft.

**Hosein Kafashan:** Writing – review & editing.

## Data availability

The data underlying this article will be shared on reasonable request to the corresponding author.

## Declaration of competing interest

The authors declare no competing interests.

## Funding and acknowledgment

The content of this article has been derived from the research project titled “Fabrication of  $ZrB_2$ -SiC-HfB<sub>2</sub> composite and investigation of its oxidation resistance” supported by Islamic Azad University of Ahvaz.

## References

- [1] A. Rezapour, Z. Balak, Fracture toughness and hardness investigation in  $ZrB_2$ -SiC-ZrC composite, *Mater. Chem. Phys.* 241 (2020) 122284. <https://doi.org/10.1016/j.matchemphys.2019.122284>.
- [2] Y. Zhang, A. Lunghi, S. Sanvito, Pushing the limits of atomistic simulations towards ultra-high temperature: A machine-learning force field for  $ZrB_2$ , *Acta Mater.* 186 (2020) 467–474. <https://doi.org/10.1016/j.actamat.2019.12.060>.
- [3] K. Kavakeb, Z. Balak, H. Kafashan, Densification and flexural strength of  $ZrB_2$ -30 vol% SiC with different amount of HfB<sub>2</sub>, *Int. J. Refract. Met. Hard Mater.* 83 (2019) 104971. <https://doi.org/10.1016/j.ijrmhm.2019.104971>.
- [4] F. Monteverde, A. Bellosi, S. Guicciardi, Processing and properties of zirconium diboride-based composites, *J. Eur. Ceram. Soc.* 22 (2002) 279–288. [https://doi.org/10.1016/S0955-2219\(01\)00284-9](https://doi.org/10.1016/S0955-2219(01)00284-9).
- [5] Y. Liu, Y. Zu, H. Tian, J. Dai, J. Sha, Microstructure and mechanical properties of continuous carbon fiber-reinforced  $ZrB_2$ -based composites via combined electrophoretic deposition and sintering, *J. Eur. Ceram. Soc.* 41 (2021) 1779–1787. <https://doi.org/10.1016/j.jeurceramsoc.2020.10.044>.
- [6] B. Feng, A. Fetzer, A.S. Ulrich, M. Christian Galetz, H. Kleebe, E. Ionescu, Monolithic  $ZrB_2$ -based UHTC s using polymer-derived Si( $Zr,B$ )CN as sintering aid, *J. Am. Ceram. Soc.* 105 (2022) 99–110. <https://doi.org/10.1111/jace.18038>.
- [7] S.D. Oguntuyi, O.T. Johnson, M.B. Shongwe, Spark plasma sintering of ceramic matrix composite of  $ZrB_2$  and TiB<sub>2</sub>: microstructure, densification, and mechanical properties-A review, *Met. Mater. Int.* 27 (2021) 2146–2159. <https://doi.org/10.1007/s12540-020-00874-8>.
- [8] M. Vajdi, S. Mohammad Bagheri, F. Sadegh Moghanlou, A. Shams Khorrami, Numerical investigation of solar collectors as a potential source for sintering of  $ZrB_2$ , *Synth. Sinter.* 1 (2021) 76–84. <https://doi.org/10.53063/synsint.2021.128>.
- [9] S. Mandal, S. Chakraborty, P. Dey, A study of mechanical properties and WEDM machinability of spark plasma sintered  $ZrB_2$ -B<sub>4</sub>C ceramic composites, *Micron.* 153 (2022) 103198. <https://doi.org/10.1016/j.micron.2021.103198>.

- [10] O. Popov, J. Vleugels, E. Zeynalov, V. Vishnyakov, Reactive hot pressing route for dense ZrB<sub>2</sub>-SiC and ZrB<sub>2</sub>-SiC-CNT ultra-high temperature ceramics, *J. Eur. Ceram. Soc.* 40 (2020) 5012–5019. <https://doi.org/10.1016/j.jeurceramsoc.2020.07.039>.
- [11] D. Zhang, P. Hu, S. Dong, C. Fang, J. Feng, X. Zhang, Microstructures and mechanical properties of Cf/ZrB<sub>2</sub>-SiC composite fabricated by nano slurry brushing combined with low-temperature hot pressing, *J. Alloys Compd.* 789 (2019) 755–761. <https://doi.org/10.1016/j.jallcom.2019.03.147>.
- [12] J. Watts, G. Hilmas, W.G. Fahrenholtz, Mechanical Characterization of ZrB<sub>2</sub>-SiC Composites with Varying SiC Particle Sizes, *J. Am. Ceram. Soc.* 94 (2011) 4410–4418. <https://doi.org/10.1111/j.1551-2916.2011.04885.x>.
- [13] R. Eatemadi, Z. Balak, Investigating the effect of SPS parameters on densification and fracture toughness of ZrB<sub>2</sub>-SiC nanocomposite, *Ceram. Int.* 45 (2019) 4763–4770. <https://doi.org/10.1016/j.ceramint.2018.11.169>.
- [14] M. Jaber Zamharir, M. Zakeri, M. Razavi, Challenges toward applying UHTC-based composite coating on graphite substrate by spark plasma sintering, *Synth. Sinter.* 1 (2021) 202–210. <https://doi.org/10.53063/synsint.2021.1452>.
- [15] J. Watts, G. Hilmas, W.G. Fahrenholtz, Mechanical characterization of ZrB<sub>2</sub>-SiC composites with varying SiC particle sizes, *J. Am. Ceram. Soc.* 94 (2011) 4410–4418. <https://doi.org/10.1111/j.1551-2916.2011.04885.x>.
- [16] S. Henderson, W.G. Fahrenholtz, G.E. Hilmas, J. Marschall, High-velocity impact resistance of ZrB<sub>2</sub>-SiC, *Mechanical Properties and Performance of Engineering Ceramics II: Ceramic Engineering and Science Proceedings*, John Wiley & Sons. (2006) 3–9. <https://doi.org/10.1002/9780470291313.ch1>.
- [17] A.L. Chamberlain, W.G. Fahrenholtz, G.E. Hilmas, Low-temperature densification of zirconium diboride ceramics by reactive hot pressing, *J. Am. Ceram. Soc.* 89 (2006) 3638–3645. <https://doi.org/10.1111/j.1551-2916.2006.01299.x>.
- [18] Y. Gupta, B.V. Manoj Kumar, ZrB<sub>2</sub>-SiC composites for sliding wear contacts: Influence of SiC content and counterbody, *Ceram. Int.* 48 (2022) 14560–14567. <https://doi.org/10.1016/j.ceramint.2022.01.349>.
- [19] S. Guo, Effects of VC additives on densification and elastic and mechanical properties of hot-pressed ZrB<sub>2</sub>-SiC composites, *J. Mater. Sci.* 53 (2018) 4010–4021. <https://doi.org/10.1007/s10853-017-1850-7>.
- [20] E.P. Simonenko, N.P. Simonenko, V.G. Sevastyanov, N.T. Kuznetsov, ZrB<sub>2</sub>/HfB<sub>2</sub>-SiC ultra-high-temperature ceramic materials modified by carbon components: the review, *Russ. J. Inorg. Chem.* 63 (2018) 1772–1795. <https://doi.org/10.1134/S003602361814005X>.
- [21] E. Dodi, Z. Balak, H. Kafashan, HfB<sub>2</sub>-doped ZrB<sub>2</sub>-30 vol.% SiC composites: oxidation resistance behavior, *Mater. Res. Express.* 8 (2021) 045605. <https://doi.org/10.1088/2053-1591/abdf1a>.
- [22] S.M. Arab, M. Shahedi Asl, M. Ghassemi Kakroudi, B. Salahimehr, K. Mahmoodipour, On the oxidation behavior of ZrB<sub>2</sub>-SiC-VC composites, *Int. J. Appl. Ceram. Technol.* 18 (2021) 2306–2313. <https://doi.org/10.1111/ijac.13858>.
- [23] L. He, Y. Sun, Q. Meng, B. Liu, J. Wu, X. Zhang, Enhanced oxidation properties of ZrB<sub>2</sub>-SiC composite with short carbon fibers at 1600 °C, *Ceram. Int.* 47 (2021) 15483–15490. <https://doi.org/10.1016/j.ceramint.2021.02.114>.
- [24] A. Vinci, L. Zoli, D. Sciti, Influence of SiC content on the oxidation of carbon fibre reinforced ZrB<sub>2</sub>/SiC composites at 1500 and 1650 °C in air, *J. Eur. Ceram. Soc.* 38 (2018) 3767–3776. <https://doi.org/10.1016/j.jeurceramsoc.2018.04.064>.
- [25] R. Inoue, Y. Arai, Y. Kubota, Y. Kogo, K. Goto, Initial oxidation behaviors of ZrB<sub>2</sub>-SiC-ZrC ternary composites above, *J. Alloy. Compd.* 731 (2018) 310–317. <https://doi.org/10.1016/j.jallcom.2017.10.034>.
- [26] C. Li, Y. Niu, T. Liu, L. Huang, X. Zhong, et al., Effect of WB on oxidation behavior and microstructure evolution of ZrB<sub>2</sub>-SiC coating, *Corros. Sci.* 155 (2019) 155–163. <https://doi.org/10.1016/j.corsci.2019.04.034>.
- [27] H. Aghajani, E. Hadavand, N.-S. Peighambari, S. Khameneh-asl, Electro spark deposition of WC-TiC-Co-Ni cermet coatings on St52 steel, *Surf. Interfaces.* 18 (2020) 100392. <https://doi.org/10.1016/j.surf.2019.100392>.
- [28] F. Sadegh Moghanlou, M. Vajdi, M. Sakkaki, S. Azizi, Effect of graphite die geometry on energy consumption during spark plasma sintering of zirconium diboride, *Synth. Sinter.* 1 (2021) 54–61. <https://doi.org/10.53063/synsint.2021.117>.
- [29] N. Sadeghi, M.R. Akbarpour, H. Aghajani, A novel two-step mechanical milling approach and in-situ reactive synthesis to fabricate TiC/Graphene layer/Cu nanocomposites and investigation of their mechanical properties, *Mater. Sci. Eng. A.* 734 (2018) 164–170. <https://doi.org/10.1016/j.msea.2018.07.101>.
- [30] R. Inoue, Y. Arai, Y. Kubota, Y. Kogo, K. Goto, Oxidation of ZrB<sub>2</sub> and its composites: a review, *J. Mater. Sci.* 53 (2018) 14885–14906. <https://doi.org/10.1007/s10853-018-2601-0>.
- [31] W.G. Fahrenholtz, The ZrB<sub>2</sub> volatility diagram, *J. Am. Ceram. Soc.* 88 (2005) 3509–3512. <https://doi.org/10.1111/j.1551-2916.2005.00599.x>.
- [32] T.A. Parthasarathy, R.A. Rapp, M. Opeka, R.J. Kerans, A model for the oxidation of ZrB<sub>2</sub>, HfB<sub>2</sub> and TiB<sub>2</sub>, *Acta Mater.* 55 (2007) 5999–6010. <https://doi.org/10.1016/j.actamat.2007.07.027>.
- [33] S.K. Thimmappa, B.R. Golla, V. Bhanu Prasad, B. Majumdar, B. Basu, Phase stability, hardness and oxidation behaviour of spark plasma sintered ZrB<sub>2</sub>-SiC-Si<sub>3</sub>N<sub>4</sub> composites, *Ceram. Int.* 45 (2019) 9061–9073. <https://doi.org/10.1016/j.ceramint.2019.01.243>.
- [34] B.R. Golla, S.K. Thimmappa, Comparative study on microstructure and oxidation behaviour of ZrB<sub>2</sub>-20 vol% SiC ceramics reinforced with Si<sub>3</sub>N<sub>4</sub>/Ta additives, *J. Alloys Compd.* 797 (2019) 92–100. <https://doi.org/10.1016/j.jallcom.2019.05.097>.
- [35] J. Zhang, H. Chen, G. Xiao, M. Yi, Z. Chen, et al., Effects of Si<sub>3</sub>N<sub>4</sub> and WC on the oxidation resistance of ZrB<sub>2</sub>/SiC ceramic tool materials, *Ceram. Int.* 48 (2022) 8097–8103. <https://doi.org/10.1016/j.ceramint.2021.12.011>.
- [36] Y. Kubota, H. Tanaka, Y. Arai, R. Inoue, Y. Kogo, K. Goto, Oxidation behavior of ZrB<sub>2</sub>-SiC-ZrC at 1700 °C, *J. Eur. Ceram. Soc.* 37 (2017) 1187–1194. <https://doi.org/10.1016/j.jeurceramsoc.2016.10.034>.
- [37] Z. Xu, F. Li, Y. Wang, K. Zhao, Y. Tang, Microstructure and oxidation resistance of ZrB<sub>2</sub>-ZrC-SiC composite nanofibers fabricated via electrospinning combined with carbothermal reduction, *Ceram. Int.* 47 (2021) 20740–20744. <https://doi.org/10.1016/j.ceramint.2021.03.317>.
- [38] Z. Xu, K. Zhao, F. Li, Y. Huo, Y. Tang, The oxidation behavior of ZrB<sub>2</sub>-ZrC composite nanofibers fabricated by electrospinning and carbothermal reduction, *Ceram. Int.* 46 (2020) 10409–10415. <https://doi.org/10.1016/j.ceramint.2020.01.039>.
- [39] X. Jin, P. Li, C. Hou, X. Wang, X. Fan, et al., Oxidation behaviors of ZrB<sub>2</sub> based ultra-high temperature ceramics under compressive stress, *Ceram. Int.* 45 (2019) 7278–7285. <https://doi.org/10.1016/j.ceramint.2019.01.009>.
- [40] W.G. Fahrenholtz, Thermodynamic analysis of ZrB<sub>2</sub>-SiC oxidation: formation of a SiC-depleted region, *J. Am. Ceram. Soc.* 90 (2007) 143–148. <https://doi.org/10.1111/j.1551-2916.2006.01329.x>.
- [41] P.A. Williams, R. Sakidja, J.H. Perepezko, P. Ritt, Oxidation of ZrB<sub>2</sub>-SiC ultra-high temperature composites over a wide range of SiC content, *J. Eur. Ceram. Soc.* 32 (2012) 3875–3883. <https://doi.org/10.1016/j.jeurceramsoc.2012.05.021>.
- [42] M. Dehghanzadeh Alvari, M. Ghassemi Kakroudi, B. Salahimehr, R. Alaghmandfard, M. Shahedi Asl, M. Mohammadi, Microstructure, mechanical properties, and oxidation behavior of hot-pressed ZrB<sub>2</sub>-SiC-B<sub>4</sub>C composites, *Ceram. Int.* 47 (2021) 9627–9634. <https://doi.org/10.1016/j.ceramint.2020.12.101>.